Structure of the most conserved internal loop in SRP RNA

Uli Schmitz[1], Thomas L. James[1], Peter Lukavsky[1,4] and Peter Walter[2,3]

Departments of [1]Pharmaceutical Chemistry and [2]Biochemistry and Biophysics, and [3]Howard Hughes Medical Institute, University of California San Francisco, 513 Parnassus, San Francisco, CA 94143-0446 [4]current address: Department of Structural Biology, Stanford University School of Medicine, Stanford, CA 94305-5400

The signal recognition particle (SRP) directs translating ribosomes to the protein translocation apparatus of endoplasmic reticulum (ER) membrane or the bacterial plasma membrane. SRP is universally conserved, and in procaryotes consists of two essential subunits, SRP RNA and SRP54, the latter of which binds to signal sequences on the nascent protein chains. Here we describe the solution NMR structure of a 28mer RNA comprising the most conserved part of SRP RNA to which SRP54 binds. Central to this function is a six nucleotide internal loop which assumes a novel Mg^{2+}-dependent structure with unusual cross-strand interactions; besides a cross-strand A/A stack, two guanines form hydrogen bonds with opposite strand phosphates. The structure completely explains the phylogenetic conservation of the loop bases, underlining its importance for SRP54 binding and SRP function.

The signal recognition particle (SRP) assumes a key role in the catalytic process of co-translational protein targeting and translocation[1]. In mammalian SRP, six proteins are bound to SRP RNA (7SL RNA) forming an extended complex with a rod-like shape[2]. Through phylogenetic comparison, SRP RNA has been divided into four structural domains (I-IV)[3], of which domain IV is the only one that is found in all of the numerous SRP RNA homologues[4]. The three functional steps of SRP-mediated protein translocation, (i) signal sequence recognition, (ii) nascent chain elongation arrest, (iii) targeting of the SRP/ribosome complex to the SRP-receptor, have been mapped to unique RNA domains and the associated proteins[1]. The interaction of SRP with the signal sequence and the SRP-receptor is intricately linked to the conserved RNA domain IV and its protein associate SRP54. The SRP homologue of *E. coli*, comprised of 4.5S RNA and a single protein, the SRP54 homologue (Ffh) (Fig. 1a), exhibits not only significant sequence conservation[3] compared to its eukaryotic relatives, but also functional similarity[5,6]. Consequently, the *E. coli* homologue is very suitable for elucidating the structural basis of signal sequence recognition and targeting to the SRP-receptor[7].

SRP54 and its homologues exhibit two proteolytically separable domains, whose crystal structures have been solved for *T. aquaticus* [8,9]*;* the N-terminal domain[8] is thought to be primarily involved in the GTP-dependent interaction with the SRP-receptor whereas the other, methionine-rich domain (FfhM)[9] is involved in signal sequence recognition and SRP RNA binding. For the latter interaction, it has been suggested for the *E. coli* system that 4.5S RNA enhances the structural stability of FfhM when it interacts with the peptide signal sequence[10]. RNA protein contacts mostly involve the internal loop regions in domain IV and RNA oligonucleotides containing only domain IV sequences bind to FfhM with roughly the same affinity as the entire 4.5S RNA (K_{Diss}: 5-20 nM)[11]. Even a 24-nucleotide fragment (residues 43-66) containing only the most conserved internal loop (C46-A47-G48/G61-C62-A63) exhibits a high, specific affinity for FfhM which suggests that the most significant element of the FfhM/domain IV recognition site is associated with this particular internal loop.

We have utilized nuclear magnetic resonance (NMR) to determine the solution structure of this domain IV fragment, containing the internal loop and a closing GGAA-tetraloop (Fig. 1b) under physiologically relevant conditions. To increase the stability of the hairpin, the terminal stem of the original *E. coli* sequence (residues 43-66) has been extended by two G:C base pairs (Fig. 1b). Earlier work[11,12] had shown that the structure of the internal loop is neither very stable nor well-defined under commonly employed

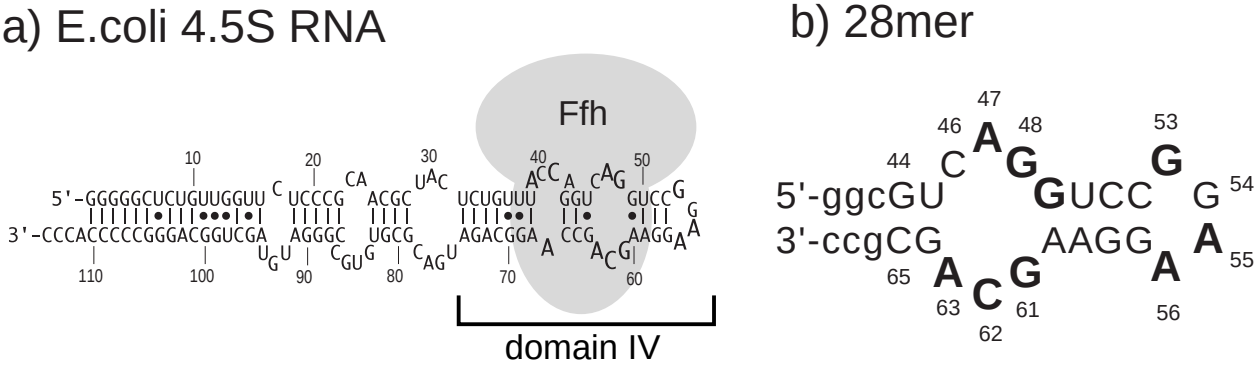

Fig. 1 a) Secondary structure of E. coli 4.5S RNA and its interaction site with Ffh (shown in gray as two domain model). **b)** 28mer hairpin sequence used for NMR structure determination. (Numbering is according to 4.5S RNA3. Non-native nucleotides are in lower case letters.) Phylogenetically conserved nucleotides are shown in bold type

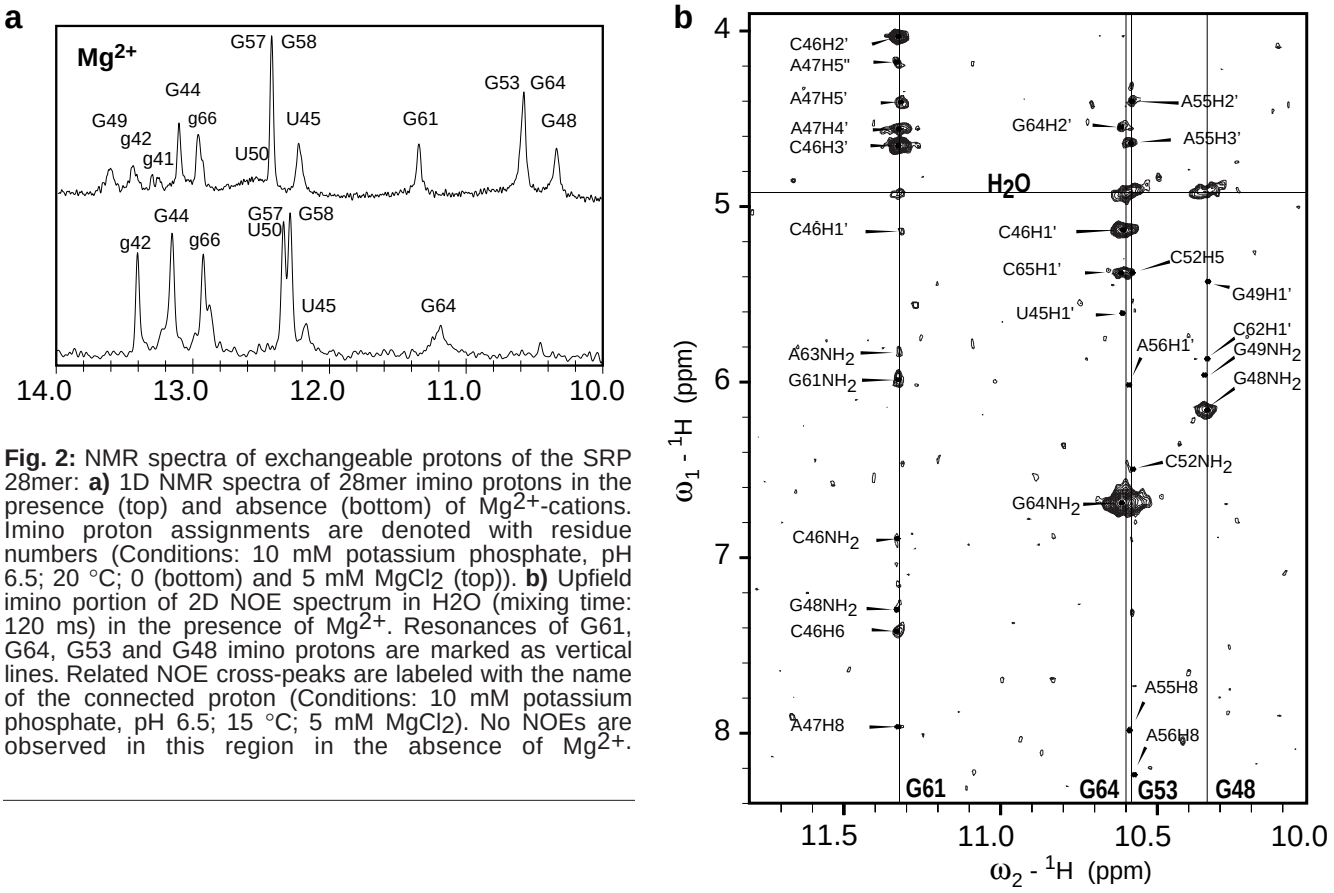

Fig. 2: NMR spectra of exchangeable protons of the SRP 28mer: **a)** 1D NMR spectra of 28mer imino protons in the presence (top) and absence (bottom) of Mg^{2+}-cations. Imino proton assignments are denoted with residue numbers (Conditions: 10 mM potassium phosphate, pH 6.5; 20 °C; 0 (bottom) and 5 mM $MgCl_2$ (top)). **b)** Upfield imino portion of 2D NOE spectrum in H2O (mixing time: 120 ms) in the presence of Mg^{2+}. Resonances of G61, G64, G53 and G48 imino protons are marked as vertical lines. Related NOE cross-peaks are labeled with the name of the connected proton (Conditions: 10 mM potassium phosphate, pH 6.5; 15 °C; 5 mM $MgCl_2$). No NOEs are observed in this region in the absence of Mg^{2+}.

conditions (i.e., 10 mM K_2HPO_4, pH 5-7, 50-100 mM NaCl). However, in the presence of physiological concentrations of Mg^{2+} (2-5 mM), the hairpin structure is stabilized significantly. This is evident in the imino proton spectra (Fig. 2a), where the two internal loop guanine imino protons, G48NH and G61NH, emerge as new, sharp resonances, suggesting their involvement in hydrogen bonding. The same two residues also exhibited unusual H1' chemical shifts[12] as seen in Fig. 3.

Structure Determination

The structure of the 28mer was determined with conventional restrained molecular dynamics, utilizing NOE-derived distance restraints along with a number of torsion angle restraints (Table I). Complete-relaxation-matrix methods[13] were used to increase the precision of the distance bounds involving nonexchangeable protons[12]. Overall, this method applied to several NOE data sets in conjunction with the relatively large number of NOEs involving exchangeable protons led to 12 distance restraints per residue, comparable to that in studies with typical isotope-labeled RNAs [14-16].

The structural statistics (Table I) of the converged structures and the final average structure (Fig. 4) indicate that the conformation of the internal loop is among the best-defined parts of the 28mer (r.m.s.d. 0.76 Å). This is remarkable since structure refinement of the internal loop was principally driven by distance and sugar pucker restraints. To avoid unnecessary bias, no backbone torsion angles were applied for the internal loop region despite absence of unusually shifted ^{31}P-resonances beyond those of the tetraloop[17].

The internal loop residues manifest multiple cross-strand interactions

In the restrained-minimized average structure of the 28mer, the internal loop depicts a novel, well-defined motif exhibiting a number of unusual hydrogen bonds. The most striking feature is that A47 and A63 (Fig. 4b,d) form a cross-strand A/A-stack in the minor groove without involving any pairing with the cross-strand cytosines. Assignment of this geometry is largely driven by a number of unusual NOEs of A47 and A63. While both A63H2 and A63H8 show NOEs to G64H8, A63H8 also exhibits NOEs to G61H3' and C62H4', reflecting the atypical backbone conformation in this region. Also A47H2 exhibits an unusual, sequential NOE to H8 of G48. The NOE between A47H2 and its own H2' reflects the unique orientation of the A47 ribose (Fig. 4b) causing a small turn in the backbone. The displacement of the A/A-stack towards the minor groove creates continuous stacking through the internal loop (G49/G48/A47/A63/G64) and permits G61 to reach across, forming a hydrogen bond between its imino and amino protons and the phosphate group of A47 (Fig. 4b,e). This remarkable positioning of G61 is directed by a number of unusual NOEs of G61NH to ribose protons of C46 and A47 (labeled in Fig. 2b). G48NH is also protected from solvent exchange but, in contrast to G61NH, it exhibits very few NOEs to non-exchangeable protons. However, the C2'-endo conformation of the G48 ribose facilitates stretching of the backbone so G48NH forms

cross-strand hydrogen bond with the C62 phosphate (Fig. 4e). Residue G48 is pushed out towards the minor groove such that its carbonyl oxygen can interact with the G61 hydroxyl group, but the imino proton is too far away from the riboses of C62 and G61 to show any NOEs. The placement of G48 and G61 side-by-side opens the possibility for a hydrogen bond between the G48 carbonyl and the G61 amino group. However, the associated distance is 0.5-1.0 Å too large. The arrangement of the two G's explains the unusual, upfield chemical shifts of G48 and G61 H1' protons (4.78 and 4.71 ppm). These protons should experience strong ring current effects being positioned directly above or below the A47 and A60 bases, respectively. The fact that the structure can explain these rather rare H1' chemical shifts so well independently validates our structure.

Some aspects of this motif with two G's engaged in cross-strand interactions and a cross-strand A/A stack have been described for the sarcin/ricin loop of 28S ribosomal RNA[18]. For the latter, a similar A/A stack was found along with one bulged guanine engaged in a cross-strand interaction with a phosphate group. In that case, the backbone seems more distorted than in the SRP RNA, where small turns in the backbones on either side compensate, thus leading to a more regular geometry.

The two cytosines of the 28mer internal loop reside in the deepened major groove and seem to contribute to the structural stability less conspicuously. Nevertheless, the conserved C62 is engaged in a unique hydrogen bond between its amino group and the G61 phosphate. For C46, which is not phylogenetically conserved, it is no surprise that only its ribose is integral for the structural motif; the C46 hydroxyl oxygen is clearly within hydrogen bonding distance to the amino group of A63 (this structural feature led to the subsequent assignment of C46*OH* and related NOEs).

The unique internal loop motif is complemented by a flanking G:U wobble pair and a carbonyl-amino G:A pair. The latter is not strictly conserved but is found in the vast majority of species spanning a wider distance across G48 and G46 than a G:C pair could.

The structure presented here agrees well with chemical and enzymatic protection data obtained for 4.5S RNA[19]. Overall, these studies suggested that the conserved internal loop is tightly structured, as we can confirm now. However, it is the small differences observed in chemical accessibility that elegantly confirm our structure. For example, both internal loop guanines are strongly protected from chemical modification, but G61 more than G48. This agrees with the latter having an exposed amino group. A47 and A63 are easily accessible to chemical modification, explained by their exposed Watson-Crick faces. Similarly, the greater accessibility of A47 compared to A63 fits well with the 28mer structure, as A63 is more buried.

The structure and its implications for SRP RNA protein binding

The overall structure of the internal loop motif is noticeably different from A-form RNA, although

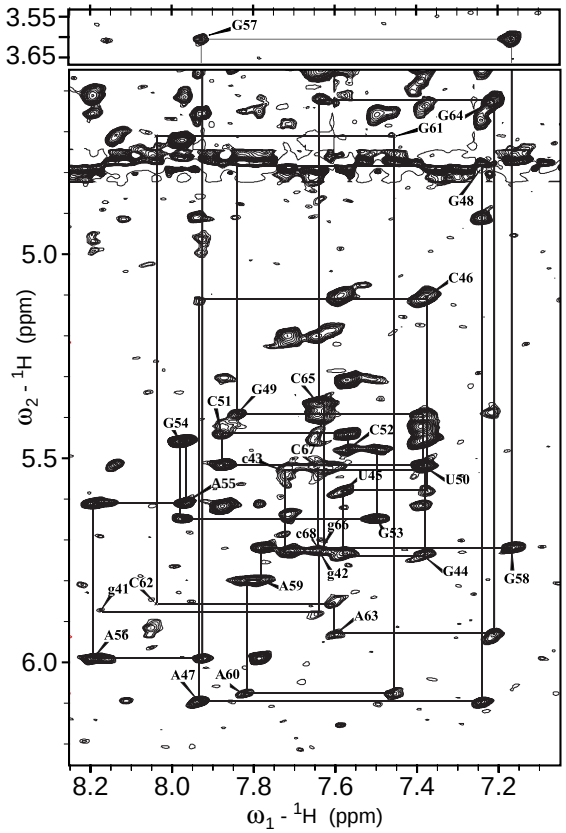

Fig 3: Portion of the 2D NOE spectrum in D2O (mixing time 200 ms) in the presence of Mg^{2+} showing aromatic to anomeric NOEs. An uninterrupted sequential H6/8-H1' walk is traced with lines where the intraresidue NOE is labeled with the residue number. (Conditions: 10 mM potassium phosphate, pH 6.5; 25 °C; 5 mM MgCl2). Note, G48, G57, G61 and G64 exhibit upfield H1'-chemical shifts.

remarkable regularity is maintained without any direct base pairing. Multiple cross-strand interactions of the purines lead to a compression of the double-helix parallel to the grooves (Fig. 4c). A similar, yet less pronounced, compression has been seen for other structures with cross-strand A/A stacks[18,20]. The surfaces in the grooves created by the conserved internal loop motif present a unique face for the interaction with proteins. For example, the minor groove is even more shallow than in A-form RNA, but exhibits an atypical patch of hydrogen bond donors (amino groups of G48 and A47; see Fig.4e) next to a larger than usual hydrophobic patch (A/A stack). Also in the major groove, the C46 and C62 amino groups stick out uniquely as hydrogen bond donors (Fig. 4b).

The most important aspect of the structure presented here, however, is that all of the phylogenetically conserved residues are involved in nucleotide specific interactions such that the phylogenetic conservation can be completely rationalized, rather than assuming that conservation reflects base-specific requirements for protein binding. The fact that Mg^{2+} is not strictly required for domain IV/FfhM binding[11] suggests that the internal loop motif is not simply a static key that fits into the protein lock. Thus, it is possible that the unique Mg^{2+}-dependent structure relates to other aspects of the RNA protein interaction than just the overall binding affinity[11], such as binding specificity or interaction kinetics.

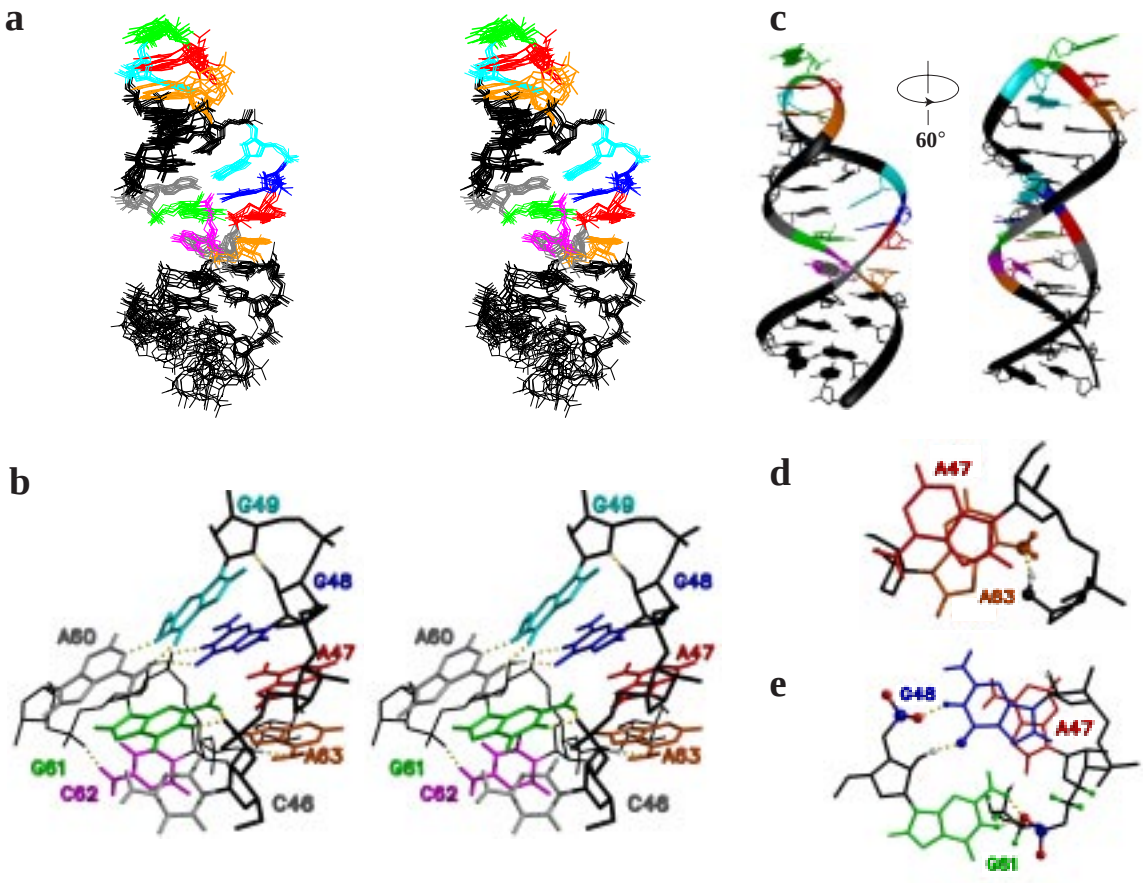

Fig. 4: The NMR structure of the SRP 28mer: **a)** Stereoview of a superposition of the seven best structures of the final ensemble. (Note, few NOEs where observed for the two terminal base pairs. Since the latter are not relevant to the conserved SRP RNA motif, no large efforts were directed towards obtaining a higher degree of convergence for this part of the molecule.) Color coding for this figure unless noted otherwise: non-conserved residues gray (C46 and A60) or black (all other); G49 and G53 cyan; G48 blue; A47 and A55 red; A63 and A56 orange; G54 and G61 green; C62 magenta. **b)** Stereoview of the conserved SRP RNA internal loop motif of the average structure. The 3'-strand with the sharper kink in the backbone is shown in back/left with a smaller linewidth. Backbones are shown in black. Hydrogen bonds as they occurred in the average structure are shown as dotted yellow lines (Beyond the G49:A60 and U45:G64 non-canonical base pairs, distances < 2.0 Å were observed for the following donor acceptor pairs (number of occurrences among the seven best structures) : i) G48HO2'-G49O4' (6), ii) G48NH-C62O1P (6), iii) G48O6-G61HO2' (7), iv) G61NH-A47O2P (6), v) G61NH2-A47O2P (4), vi) A63N6-C46HO2' (7), vii) C62NH2 -G61O2P (6)). Ribose hydrogen atoms were omitted. **c**) Two views of the final NMR structure of the 28mer in ribbon representation; view into major groove with A/A stack in the back (right); after 60° rotation (left). (The terminal base pair has been omitted.) **d)** The cross-strand stack between A47 (above) and A63 (below) and the putative A63-amino to C46-hydroxyl contact (dotted). **e**) Side-by-side47. Atoms involved in hydrogen bonds are shown as balls. The protons that exhibit NOEs to G61NH as seen in Fig. 2a are shown as green balls.

Furthermore, the significantly increased thermodynamic stability in the presence of Mg^{2+} might also reflect a role of the conserved motif in efficient folding of the SRP RNA, since the internal loop could enhance the nucleation effect of the GGAA-tetraloop.

Methods

RNA synthesis and purification. The SRP 28mer was synthesized by *in vitro* transcription using T7 RNA polymerase according to the method of Milligan *et al.*[21]. RNA from a 25 ml reaction was purified on 20% polyacrylamide/7 M urea gels similar to that described previously [11,12], yielding 110 OD_{260}.

NMR sample preparation and NMR experiments. The SRP 28mer was lyophilized several times from D_2O for analysis of nonexchangeable protons. The sample was annealed immediately prior to conducting NMR experiments by heating at 85 °C for 10 min and snap-cooling on ice for 30 min. To minimize formation of dimeric species, $MgCl_2$ was added after annealing. Final conditions for the 28mer were 0.25 mM RNA, 5 mM $MgCl_2$, 10 mM potassium phosphate at pH 6.5. For analysis of exchangeable protons, the sample was lyophilized and dissolved in 9:1 H_2O/D_2O with the same conditions as above. For acquisition of 2D NMR data we used an 8 mm Nalorac probe on a UNITYPLUS 600 MHz spectrometer.

All 2D nuclear Overhauser effect spectra (mixing times: 50, 150, 200 and 400 ms) in D_2O were acquired in the hypercomplex mode at 25 °C and 30 °C, using a spectral width of 5999 Hz in both dimensions. A total of 400 t_1 values were recorded with 32 scans per free induction decay and a repetition time of 2.5 s. Double-quantum filtered

Table I. Statistics for restraints and final structural ensemble of SRP 28mer.

Restraints		
Total distance restraints (interresidue)	336 (242)	
MARDIGRAS derived [a]	239	
qualitative, exchangeable protons [b]	97	
average number per residue:	12	
other:		
base pair restraints (dist., angle) [c]	44	
sugar pucker restraints (dihedral)	125	
backbone (dihedral) [d]	50	
Total restraint average per residue	20	
Ensemble Parameters	**<SA>[e]**	**SA[e]**
average deviations from bounds:		
all interproton distances (Å)	0.0690±0.002	0.054
all angles (degrees)	1.1±0.2	0.9
all dihedral angles (degrees)	1.2±0.7	0.2
number of distance violations > 0.4 Å [f]	6.3±0.8	3
RMSD deviation from ideal geometry		
bonds (Å)	0.013 ±0.0003	0.012
angles (degrees)	3.3±0.17	3.1
average atomic RMSD (Å)		
all nucleotides (except terminal GC)	1.27±0.32	0.90±0.34
apical part (nucl. 44-65)	1.03±0.24	0.73±0.23
tetraloop (nucl. 52-57)	0.80±0.37	0.59±0.34
symmetric bulge (nucl. 45-49, 60-64)	0.76±0.14	0.55±0.13

[a] Average width between bounds is 1.65±0.48 Å.
[b] Most bounds were set to 0-6Å; for some strong NOEs, upper bounds of 2.5 Å or 4 Å were used.
[c] Besides 7 Watson-Crick base pairs, restraints were included for the U45:G64 wobble pair and the G49:A60 N1-N1 carbonyl-imino pair.
[d] A-form backbone torsion angles (α = -62±10, β = -179±10, γ = 47±10, ε = -151±10, ζ= -73±10) were used for residues g42-G44, U50-C52, G57-A59 and C65-c68. For these residues all base-ribose connectivities typical for A-form RNA are seen along with the expected NOEs for the exchangeable protons.
[e] Seven structures were included in the final ensemble <SA> based on the evaluation of restraint violations on a per residue basis. The ensemble was averaged and restrained energy-minimized to yield the final structure SA.
[f] No violations exceed 0.6 Å. The larger violations arise mostly from the shorter MARDIGRAS-derived distances with relatively tight bounds.

correlated spectra were acquired under the same conditions. All 2D NOE experiments in H_2O were collected at 5 °C, 10 °C or 15 °C using the SSNOESY pulse sequence[22] with a spectral width of 12999 Hz using a symmetrically-shifted S-pulse with a pulse width of 88.8 μs for water suppression. Mixing times were 120 and 200 ms. Data were processed with the local software Striker and SPARKY (Copyright UCSF, San Francisco, CA, 1992).

Resonance assignments followed well-established procedures[23] and have been described previously[11,12]. Chemical shift assignments are available as supplementary material at our website http://picasso.ucsf.edu/supplement.html along with a list of distance restraints and plots of NOE data. The G48 and G61 imino assignments, cornerstones for the 28mer structure, were confirmed when no reasonable structures could be calculated with the wrong, switched assignments reported earlier[12]. Note, our ongoing work with ^{15}N,^{13}C-labeled RNA samples of the entire domain IV (43 nucleotides) confirmed the assignments for residues U45-G64 in the 28mer.

Restraint generation and refinement procedures: NOE cross-peak volumes were corrected for partial relaxation effects with the program SYMM[24]. Corrected intensities were used for all complete relaxation matrix calculations with the program MARDIGRAS (Copyright UCSF, San Francisco, CA, 1990/94). The randmardi procedure with 50 repetitions[25] and intensity errors of 5-50% was invoked for three NOESY data sets (150, 200, 400ms) using five correlation times (3.0, 3.5, 4.0, 4.5 and 5.0 ns). Final upper and lower distance bounds were calculated by adding and subtracting the standard deviation of all runs to the average upper and lower bounds from individual randmardi runs[12].

An A-form hairpin starting model for the 28mer was built with SYBYL (Tripos Associates, St. Louis, MO). The restrained MD refinement was carried out with the SANDER module of the AMBER 4.1 program suite (Copyright UCSF, San Francisco, 1995) and the Cornell *et al*. force field[26]. Structural analysis was carried out with the CARNAL module of AMBER 4.1, CURVES 5.1[27] and MidasPlus (Copyright UCSF, San Francisco, CA, 1985/89).

Our refinement protocol consisted of (i) 3-5 ps free MD with steep heating and temperature coupling from 0 to 1500K for randomization of the starting structure, (ii) 1000 steps of conjugate gradient energy-minimization of the distorted, melted structure, (iii) 3-5 ps restrained MD with temperature and restraint weight ramping up to 500K and 50 kcal/mol·Å^2 for distance and 250 kcal/mol·rad^2 for torsion angle restraints, respectively, (iv) continuation of restrained MD for 4 ps under high temperature and restraint weight conditions, (v) rescaling temperature and force-constants to 200K and 20 kcal/mol·Å^2 for distance and 100 kcal/mol·rad^2 for torsion angle restraints within 0.5 ps, after which the simulation is run out to 10 or 15 ps. For the first 5 ps of the restrained MD period, the weight of the van der Waals term was set to 0.1, ramped to 5 for 1 ps and rescaled to 1 for the remainder of the run. The weight of the electrostatics term was kept at 0 for the first 7 ps and ramped to 1 for the rest of the time. Final structures were calculated by averaging the coordinates of the last 2 ps and restrained energy-minimization with force-constants of 20 kcal/mol·Å^2 for distance and 100 kcal/mol·rad^2 for torsion angle restraints. Structures were accepted when the global average distance deviation was below 0.08 Å and the average deviation for each of the internal loop and tetraloop residues was below 0.12 Å without worsening the conformational energy more than 400 kcal/mol compared to a freely minimized structure. Seven out

of fifteen trial structures were averaged and energy-minimized with force-constants of 30 kcal/mol·Å^2 for distance and 150 kcal/mol·rad^2 for torsion angle restraints.

Coordinates have been deposited with the Protein Data Bank with accession number 28sr and 28sp.

Acknowledgments.
This research was supported by NIH grant GM39247 to TLJ and NSF grant MCB-9513214 to US. The NMR instrument was purchased with funds from NIH grant RR01490. PW is an investigator of the Howard Hughes Medical Institute. We acknowledge the UCSF Computer Graphics laboratory supported by NIH grant RR01081.

Received 18 March; accepted 30 March, 1999

1. Walter, P. & Johnson, A.E. *Ann. Rev. Cell Biol.* **10**, 87-119 (1994).
2. Andrews, D.W., Walter, P. & Ottensmeyer, F.P. *EMBO J.* **6**, 3471-3477 (1987).
3. Poritz, M.A., Strub, K. & Walter, P. *Cell* **55**, 4-6 (1988).
4. Larsen, N., Samuelsson, T. & Zwieb, C. *Nucl. Acids Res.* **26**, 177-178 (1998).
5. Bernstein, H.D., Zopf, D., Freymann, D.M. & Walter, P. *Proc. Natl. Acad. Sci. USA* **90**, 5229-5233 (1993).
6. Ulbrandt, N.D., Newitt, J.A. & Bernstein, H.D. *Cell* **88**, 187-196 (1997).
7. Powers, T. & Walter, P. *EMBO J.* **16**, 4880-4886 (1997).
8. Freymann, D.M., Keenan, R.J., Stroud, R. & Walter, P. *Nature* **385**, 361-364 (1997).
9. Keenan, R.J., Freymann, D.M., Stroud, R. & Walter, P. *Cell* **94**, 181-191 (1998).
10. Zheng, N. & Gierasch, L.M. *Mol Cell* **1**, 79-87 (1997).
11. Schmitz, U. *et al. RNA* **2**, 1213-1227 (1996).
12. Lukavsky, P., Billeci, T.M., James, T.L. & Schmitz, U. in ACS Sym. Ser.: Mol. Modeling of Nucl. Acids Vol. 682 (eds. SantaLucia, J. & Neocles, L.) 122-149 (, 1997).
13. Borgias, B.A., Gochin, M., Kerwood, D.J. & James, T.L. *Prog. in Nuc. Mag. Res. Spect.* **22**, 83-100 (1990).
14. Puglisi, E.V., Green, R., Noller, H.F. & Puglisi, J.D. *Nat. Struct. Biol.* **4**, 775-778 (1997).
15. Puglisi, E.V. & Puglisi, J.D. *Nature Structural Biology* **5**, 1033-1036 (1998).
16. Jucker, F.M., Heus, H.A., Yip, P.F., Moors, E.H.M. & Pardi, A. *J. Mol. Biol.* **264**, 968-980 (1997).
17. Legault, P. & Pardi, A. *J. Magn. Res.* **103**, 82-86 (1994).
18. Szewczak, A.A. & Moore, P.B. *J. Mol. Biol.* **247**, 81-98 (1995).
19. Lentzen, G., Moine, H., Ehresmann, B. & Wintermeyer, W. *RNA* **2**, 244-253 (1996).
20. Dallas, A. & Moore, P.B. *Structure* **5**, 1639-1653 (1997).
21. Milligan, J.F., Groebe, D.R., Witherell, G.W. & Uhlenbeck, O.C. *Nuc. Acid Res.* **15**, 8783-8798 (1987).
22. Smallcombe, S.H. *J. Am. Chem. Soc.* **115**, 4776-4785 (1993).
23. Varani, G. & Tinoco, I. *Q. Rev. Biophys.* **24**, 479-532 (1991).
24. Liu, H., Tonelli, M. & James, T.L. *J. Magn. Res.* **111**, 85-89 (1996).
25. Liu, H., Spielmann, H.P., Ulyanov, N.B., Wemmer, D.E. & James, T.L. *J. Biomol. NMR* **6**, 390-402 (1995).
26. Cornell, W., Cieplak, P., Bayly, C.I., Gould, I.R. & Kollman, P.A. *J. Am. Chem. Soc.* **118**, 2309-2309 (1996).
27. Lavery, R. & Sklenar, H. *J. Biomol. Struct. Dyn.* **6**, 655-667 (1989).